

WEIGHING THE QUIESCENT CENTRAL BLACK HOLE IN AN ELLIPTICAL GALAXY WITH X-RAY EMITTING GAS

PHILIP J. HUMPHREY¹, DAVID A. BUOTE¹, FABRIZIO BRIGHENTI^{2,3}, KARL GEBHARDT⁴ AND WILLIAM G. MATHEWS³

Accepted for publication in the Astrophysical Journal

ABSTRACT

We present a *Chandra* study of the hot ISM in the giant elliptical galaxy NGC 4649. In common with other group-centred ellipticals, its temperature profile rises with radius in the outer parts of the galaxy, from ~ 0.7 keV at 2 kpc to ~ 0.9 keV by 20 kpc. However, within the central ~ 2 kpc the trend reverses and the temperature peaks at ~ 1.1 keV within the innermost 200 pc. Under the assumption of hydrostatic equilibrium, we demonstrate that the central temperature spike arises due to the gravitational influence of a quiescent central super-massive black hole. We constrain the black hole mass (M_{BH}) to $(3.35^{+0.67}_{-0.95}) \times 10^9 M_{\odot}$ (90% confidence), in good agreement with stellar kinematics measurements. This is the first direct measurement of M_{BH} based on studies of hydrostatic X-ray emitting gas, which are sensitive to the most massive black holes, and is a crucial validation of both mass-determination techniques. This agreement clearly demonstrates the gas must be close to hydrostatic, even in the very centre of the galaxy, which is consistent with the lack of morphological disturbances in the X-ray image. NGC 4649 is now one of only a handful of galaxies for which M_{BH} has been measured by more than one method. At larger radii, we were able to decompose the gravitating mass profile into stellar and dark matter (DM) components. Unless one accounts for the DM, a standard Virial analysis of the stars dramatically over-estimates the stellar mass of the galaxy. We find the measured J-band stellar mass-to-light ratio, $1.37 \pm 0.10 M_{\odot} L_{\odot}^{-1}$, is in good agreement with simple stellar population model calculations for this object.

Subject headings: Xrays: galaxies— galaxies: elliptical and lenticular, cD— galaxies: individual (NGC4649)— black hole physics

1. INTRODUCTION

It is becoming increasingly clear that supermassive black holes (SMBHs) in the centres of galaxies are intimately involved in the evolution of their hosts. Models of galaxy formation suggest that energy injection from active galactic nucleus (AGN) outbursts, in particular during hierarchical assembly, can have a significant impact on the structure of the evolving galaxy (e.g. Silk & Rees 1998; Di Matteo et al. 2005). In galaxy groups and clusters, cavities in the hot intra-cluster medium (ICM) are a direct, observable manifestation of an episodic, AGN-driven feedback process acting on the ICM (e.g. Bîrzan et al. 2004). Such feedback has been implicated in global heating of the gas (e.g. Donahue et al. 2006), redistributing metals through the ICM (e.g. Mathews et al. 2004) and invoked as a possible solution to the “cooling paradox” (Mathews & Brighenti 2003, and references therein).

Evidence for SMBHs has been found in increasingly large numbers of non-active galactic nuclei, leading to the picture of ubiquitous SMBHs in stellar spheroids which has begun to emerge (Ferrarese & Ford 2005, for a review). The black hole mass (M_{BH}) has been found to correlate with properties of the host, such as luminos-

ity or mass of the bulge (Kormendy & Richstone 1995; Magorrian et al. 1998; McLure & Dunlop 2002; Marconi & Hunt 2003), the central light concentration (Graham et al. 2001), or the central velocity dispersion (σ_*) of the galaxy (Gebhardt et al. 2000a; Ferrarese & Merritt 2000; Tremaine et al. 2002). These observational relationships are starting to become a key constraint on galaxy-formation models (e.g. Robertson et al. 2006; Granato et al. 2004). There remain however, concerns over the exact shape of the relations. In particular, different authors have found different slopes for the $M_{\text{BH}}-\sigma_*$ relation (Tremaine et al. 2002; Ferrarese & Ford 2005), and there are suggestions it may deviate from a simple powerlaw relation (Wyithe 2006). Possible disagreement in the masses of the largest SMBHs inferred from the $M_{\text{BH}}-\sigma_*$ and M_{BH} -bulge luminosity relations (Lauer et al. 2007) raise questions over which relation is more fundamental. Clearly, further progress requires a careful assessment of possible systematic biases in the black hole mass measurements, especially in the high-mass regime.

A few independent techniques have evolved to measure the masses of SMBHs, each relying on its own set of simplifying assumptions. In galaxies with quiescent nuclei, the presence of the black hole is measured by its gravitational influence on the kinematics of either the stars or, if present, a central ionized gas disk (e.g. Gebhardt et al. 2003; Macchetto et al. 1997). Since gas disks are not found in every galaxy, stellar kinematical studies, based on measuring the line-of-sight velocity dispersion profile are more generally applicable. Such studies are, however, complicated by a strong degeneracy between orbital structure and the gravitating mass profile, par-

¹ Department of Physics and Astronomy, University of California at Irvine, 4129 Frederick Reines Hall, Irvine, CA 92697-4575

² Dipartimento di Astronomia, Università di Bologna, Via Ranzani 1, Bologna 40127, Italy

³ University of California Observatories, Lick Observatory, University of California at Santa Cruz, Santa Cruz, CA 95064

⁴ Astronomy Department, University of Texas, Austin, TX 78712

ticularly in slowly-rotating galaxies (Binney & Mamon 1982). Although measuring high-order moments of the velocity dispersion profile allows the degeneracy to be partially broken (van der Marel & Franx 1993), the solution is not, in general, unique (Valluri et al. 2004). To obtain interesting constraints on the SMBH mass, therefore, additional constraints such as a restricted range of allowed orbits or smoothly-varying phase-space are required (e.g. Magorrian et al. 1998; Gebhardt et al. 2003). If these assumptions are unrepresentative, however, Valluri et al. pointed out that the systematic errors in the M_{BH} determination can exceed the statistical errors.

Given the good agreement in the shape of the $M_{\text{BH}}-\sigma_*$ relation measured using masses obtained with different methods (e.g. Gebhardt et al. 2000b; Ferrarese et al. 2001), it seems unlikely that SMBH masses determined from state-of-the-art “3-integral” methods (van der Marel et al. 1998; Gebhardt et al. 2003) are *on average* in error. Nevertheless, a proper assessment of the systematics inherent in the mass determination, by comparing masses *for the same black hole* measured using different techniques is of considerable importance. To date there are only a handful of galaxies for which recent stellar kinematical M_{BH} measurements have been compared with at least one reliable, independent technique. Stellar and gas dynamical estimates of M_{BH} have been found to agree reasonably in at least two systems, NGC 3379 and Cen A (Shapiro et al. 2006; Marconi et al. 2006), although there is evidence of non-circular motions in NGC 3379, which can lead to a systematically misestimated M_{BH} . Similar agreement has been found for M 81 (Kormendy 2004), although the stellar kinematics measurement was based on “2-integral” models, which are potentially unreliable as they place constraints on the orbital structure which appear unrealistic, such as assuming the orbits are described entirely by only two integrals of motion (for more discussion see Ferrarese & Ford 2005). Non-circular gas motions may explain strong discrepancies between M_{BH} measured by these different techniques in the galaxies IC 1459 and NGC 4335 (Cappellari et al. 2002; Verdoes Kleijn et al. 2002). Despite this concern, the $M_{\text{BH}}-\sigma_*$ relation is usually constructed by combining samples of galaxies in which M_{BH} has been determined from stellar kinematics and samples for which gas dynamics has been used (e.g. Tremaine et al. 2002), and there is little evidence that the sub-samples obey appreciably different relations.

Other methods of determining M_{BH} are available in galaxies containing active galactic nuclei (AGNs), such as measuring the motions of masing gas (Miyoshi et al. 1995) or “reverberation mapping”, using the variability of the AGN (e.g. Peterson et al. 2004). In two cases M_{BH} determined from reverberation mapping has been compared to stellar kinematics results (Davies et al. 2006; Onken et al. 2007), but since the uncertainties in the former technique lead to masses accurate only to within a factor of ~ 3 (Onken et al. 2004), these measurements do not provide good constraints on the validity of the stellar models.

A new method to identify SMBHs in giant elliptical galaxies was suggested by Brighenti & Mathews (1999), who pointed out that the gravitational influence of a central black hole should have an impact on the distribution of the characteristically hot interstellar medium (ISM).

The ISM should gradually flow inwards as it loses energy from the emission of thermal X-rays but, since the local cooling time far exceeds the local free-fall timescale, the flow is highly subsonic and the gas remains close to hydrostatic equilibrium (Mathews & Brighenti 2003). In the powerful gravitational field close to the black hole, the inflowing gas should be sufficiently compressed to cause a strong temperature peak, which could be used as a black hole diagnostic. However, detections of central temperature peaks in galaxies are rare (Humphrey et al. 2004; Humphrey & Buote 2006a; Humphrey et al. 2006) and this hypothesis has, therefore, yet to be verified observationally. In part this reflects the difficulty in obtaining precise temperature constraints from X-ray spectroscopy on scales of a few hundred parsecs. AGN-induced disturbances are also common in the centres of early-type galaxies (Jones et al. 2002; Birzan et al. 2004) and these may disturb the gas enough to destroy many such hot cores.

In this paper, we present a detailed *Chandra* study of NGC 4649, a nearby, very relaxed and X-ray bright galaxy which is arguably the most promising candidate in which to search for this effect. Based on stellar kinematical studies, Gebhardt et al. (2003) reported a black hole mass of $(2.0^{+0.4}_{-0.6}) \times 10^9 M_\odot$ ($1-\sigma$ errors), placing it at the upper end of the $M_{\text{BH}}-\sigma_*$ relation. A modest archival *Chandra* dataset has already revealed a remarkably relaxed X-ray morphology (implying hydrostatic equilibrium is a good approximation: Buote & Tsai 1995) and a temperature profile which peaks in the centre (Humphrey et al. 2006; Randall et al. 2004). The object is faint in the radio (Condon et al. 2002), indicating that it does not host a powerful AGN, and there is little evidence of morphological disturbances indicating AGN-ISM interaction (§ 2.1). On a large scale, excellent agreement between the mass determined from globular cluster kinematics and X-ray methods (Bridges et al. 2006) also provides good support for hydrostatic equilibrium. We present deep new data which enable us to obtain interesting temperature constraints on scales as small as ~ 150 pc, which is crucial given the ~ 60 pc sphere of influence of the SMBH on the gas⁵. For the first time in *any* system we are able to place constraints on M_{BH} from hydrostatic X-ray gas.

We adopted a nominal distance of 15.6 Mpc for NGC 4649, based on the I-band SBF distance modulus estimate of Tonry et al. (2001), which was corrected by -0.16 to account for recent revisions to the Cepheid zero-point. At this distance, $1''$ corresponds to 76 pc. Unless otherwise stated, all error-bars represent 90% confidence limits.

2. X-RAY DATA ANALYSIS

The region of sky containing NGC 4649 has been imaged by the *Chandra* ACIS instrument in ACIS-S configuration on three separate occasions, as listed in Table 1. We processed each dataset independently, using the *CIAO* 3.4 and *Heasoft* 5.3.1 software suites, in conjunction with *Chandra* calibration database (*Caldb*) version 3.3.0.1. To ensure up-to-date calibration, all data

⁵ Defined as GM_{BH}/c_s^2 , where c_s is the central gas sound-speed (in the absence of a black hole), $\sim 490 \text{ km s}^{-1}$ from our data. This is slightly smaller than the sphere of influence on the stars, $GM_{\text{BH}}/\sigma_*^2$, which is ~ 100 pc for the measured $\sigma_* = 385 \text{ km s}^{-1}$ (Gebhardt et al. 2003).

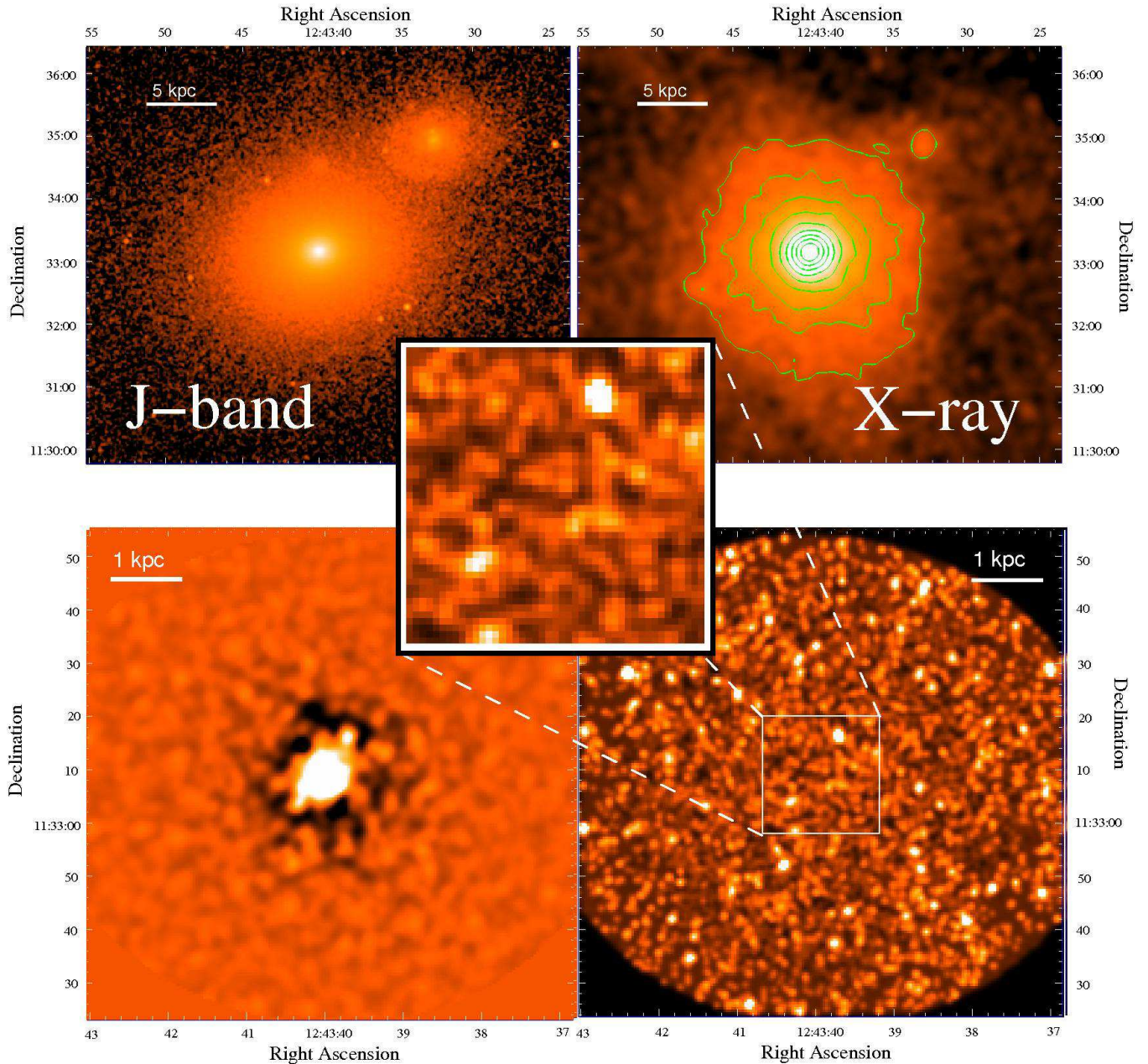


FIG. 1.— *Top left*: J-band 2MASS image of NGC 4649. Note the interloper spiral galaxy NGC 4647 to the northwest. *Top Right*: point-source cleaned *Chandra* image of NGC 4649, smoothed by a 5'' Gaussian kernel, shown with arbitrary, logarithmically-spaced contours. Note there is only a small amount of emission apparently associated with NGC 4647. *Bottom left*: “Unsharp-masked” *Chandra* image of the central part of NGC 4649 (note the different scale), created by subtracting an image smoothed with a 3'' Gaussian kernel from one smoothed by a 1'' kernel. The dark ring around the central, bright emission is an artefact of the smoothing process. *Bottom right*: “residual significance” image (see text) of the central part of the galaxy, indicating deviations from a model derived from elliptical isophote fitting to the data. The galaxy is very relaxed at all scales, and we do not confirm recent suggestions of morphological disturbances. *Center*: central 22'' \times 22'' region of the residual significance image.

were reprocessed from the “level 1” events files, following the standard *Chandra* data-reduction threads⁶. We applied the standard correction to take account of the time-dependent gain-drift and charge transfer inefficiency, as implemented in the *CIAO* tools. To identify periods of enhanced background (“flaring”), which seriously degrades the signal-to-noise (S/N) we accumulated background lightcurves for each dataset from low surface-brightness regions of the active chips, excluding

obvious point-sources. Periods of flaring were identified by eye and excised. The final exposure times are listed in Table 1.

2.1. X-ray image

For each dataset we generated a full resolution image in the 0.3–7.0 keV energy-band and a corresponding exposure map computed at an energy of 1.7 keV. Point sources were detected in each image with the *CIAO* `wavdetect` task, which was set to search for structure at scales of 1, 2, 4, 8 and 16 pixels, and supplied with the

⁶ <http://cxc.harvard.edu/ciao/threads/index.html>

TABLE 1
OBSERVATION SUMMARY

ObsID	Start Date	Exposure (ks)
785	2000 Apr 20	18
8182	2007 Jan 31	48
8507	2007 Feb 1	15
Total	...	81

NOTE. — Details of the *Chandra* observations used in the present analysis. For each dataset we quote the observation ID number (ObsID), the start date and the exposure time, having removed periods of background “flaring” (Exposure)

exposure-maps to minimize spurious detections at the image boundaries. The detection threshold was set to 10^{-6} , corresponding to $\lesssim 1$ spurious source detections per chip. To improve the signal-to-noise (S/N) of the data, we combined the resulting images and exposure maps. Given errors in the absolute astrometry of *Chandra*, we corrected the aspect onto a common frame of reference before addition. To achieve this registration, we matched common point-sources in each image and shifted the data to ensure the maximum number of such sources overlapped. Since there can be variability in a significant fraction of the LMXBs in any galaxy (or, indeed, in background AGN) we did not require all point sources to match. Having generated a merged image and exposure-map, to improve signal-to-noise (S/N), we re-detected the point sources. All detected sources were confirmed by visual inspection, and, for each, appropriate elliptical regions containing approximately 99% of its photons were generated.

We examined the image for evidence of morphological disturbances which may suggest deviations from hydrostatic equilibrium. First we processed each image to remove the point-sources. To do this, we replaced all photons within the source detection ellipse of each source with artificial data, using the algorithm described in detail in Fang et al. (2008). In short, since the **wavdetect** task can be used to generate a smoothed, “normalized” source-free image, we replaced the data within each source detection ellipse from our real image with data from the corresponding pixels on the source-free image, after adding Poisson noise and taking exposure-map variations into account. We found this procedure generally worked extremely well at removing sources. The data were then flat-fielded with the exposure map and examined by eye. We show in Fig 1 the image of NGC 4649, having smoothed it slightly with a $5''$ (0.4 kpc) Gaussian kernel. The image is remarkably round and shows no evidence of disturbances or structure. It is interesting to note that the X-ray image is rounder than the optical light (which is, nonetheless, quite round, with a major/minor axis ratio of $\lesssim 1.2$). This is unsurprising since gas in hydrostatic equilibrium traces the *potential* (the “X-ray shape theorem”: Buote & Canizares 1994), which is rounder than the mass distribution giving rise to it.

To seek evidence of more subtle structure, we experimented with “unsharp masking” the image, i.e. differencing the image smoothed at two different scales. We did not find convincing evidence of any morphological disturbances for any of the scales (using smoothing ker-

nels from $3\text{--}20''$) we tried. We show in Fig 1 a typical “unsharp-masked” image, illustrating the lack of sub-structure (note that the dark ring around the central bright region is an artefact of the smoothing process). Shurkin et al. (2008) recently argued for the presence of AGN-induced cavities in the centre of NGC 4649, but, using deeper data than these authors, we found little evidence for such features. Performing the “unsharp masking” they describe, we found little evidence for the supposed cavities, save features which are practically indistinguishable from erratic structure arising as an artefact of the image processing. Nonetheless, to assess whether any such depressions do exist, we first fitted elliptical isophotes to the central part of the X-ray image with the *PC-IRAF* task **ellipse**. We then extracted the total counts both in the image and the model within two circular apertures of $4''$ diameter placed approximately at the positions reported by Shurkin et al. (2008) for the depressions. One can then compute $\chi^2 = (\text{data-model})^2 / \text{model}$ which can be used to assess the significance of the features. A standard χ^2 would assume that we had performed a random trial, however, which is clearly incorrect here. Instead, we performed Monte-Carlo simulations to assess the true distribution of χ^2 . We performed 1000 such simulations, in each of which an artificial image was generated by adding Poisson noise to the model image. The model was then subtracted and the resulting image smoothed (with a $2''$ Gaussian) to bring out low counts structure at the scale of interest which lay close to the apparent north and south radio lobes (by which we mean within $25'' \times 25''$ boxes centred on each lobe). We repositioned the circular apertures at the corresponding minima and computed χ^2 from the (unsmoothed) artificial data. We found that 5.3% of the simulations gave χ^2 larger than we obtained with the real data, implying that the putative cavities are significant only at $\lesssim 2\text{-}\sigma$. We therefore consider the evidence for AGN-induced cavities in the hot gas to be weak.

To investigate the presence of other possible structures, we show in Fig 1 an indication of deviations from our model fit by plotting $(\text{data-model})^2 / \text{model}$, which corresponds to the χ^2 residual in each pixel. To bring out structure, we smoothed this image with a Gaussian kernel of width $0.5''$ (1 pixel). As is clear from this “residuals significance” image, there is no evidence of any coherent residual features (with the possible exception of one or two point-sources that may have been imperfectly removed). The X-ray emission is therefore very smooth and symmetric.

Randall et al. (2006, 2004) adaptively smoothed *Chandra* and *XMM* images of NGC 4649 (using shallower *Chandra* data than the present work) and identified radial features they dubbed as “fingers of emission”. However, although adaptive smoothing can give a useful overall impression of the data, it tends to introduce artificial structure into images. Our data are deeper and we do not find convincing evidence of such features. Furthermore, visual comparison of the authors’ *Chandra* and *XMM* images suggests some differences; in particular the radially-averaged, azimuthal surface-brightness plots do not obviously resemble each other, with the *XMM* data appearing (by eye) to show a larger amplitude variation with position angle than the *Chandra* data. Since *XMM* is less

able to resolve out LMXBs, we speculate that unresolved point-sources may be largely responsible for the significant structure reported for the *XMM* data. Even taking the supposed *XMM* structures at face value, they would imply azimuthal variations in gas density of only $\sim 5\%$. Small variations of this magnitude do not constitute significant deviations from hydrostatic equilibrium and are smaller, in general, than our measurement errors. Based on the shallower observation, Randall et al. (2004) also report a $\sim 2.5\text{-}\sigma$ detection of a central $\sim 5''$ structure, but inspection of the “residual significance” image shown in Fig 1 indicates there are no significant residual structures in the central region.

2.2. Spectral analysis

We extracted spectra in a series of concentric, contiguous annuli, placed at the X-ray centroid. We determined the centroid iteratively by placing a $0.5'$ radius aperture at the nominal galaxy position (obtained from *NED*) and computing the X-ray centroid within it. The aperture was moved to the newly-computed centroid, and the procedure repeated until the computed position converged. The widths of the annuli were chosen so as to contain approximately the same number of background-subtracted photons, and ensure there were sufficient photons to perform useful spectral-fitting (in this case we had $\gtrsim 2000$ background-subtracted photons per spectrum). We placed a lower limit of $2.5''$ on the annulus width, to ensure that the instrumental spatial resolution does not lead to strong mixing between the spectra in adjacent annuli. The data in the vicinity of any detected point source were excluded, as were the data from the vicinity of chip gaps, where the instrumental response may be uncertain. To prevent possible low-level contamination from any hot gas in the central part of the interloper galaxy NGC 4647, we additionally excluded data in its vicinity from the $9.3\text{--}13.1$ kpc annulus, which intersects its centre. We extracted products from all active chips, excluding the S4 (which suffers from considerable “streaking” noise). Appropriate count-weighted spectral response matrices were generated for each annulus using the standard *CIAO* tasks *mkwarf* and *mkacisrmf*. For each spectrum, we estimated the background using the method outlined in Humphrey et al. (2006). We extracted identical products individually for each dataset, taking into account the astrometric offsets between them (determined from the image registration discussed above). The source and background spectra were added, and the response matrices averaged using the standard *Heasoft* tasks *addrmf* and *addarf*, with weights based on the number of photons in each spectrum. We found there was very little emission outside $\sim 5'$ (23 kpc), indicating truncation of the X-ray halo outside this radius as NGC 4649 falls into the Virgo cluster.

Spectral-fitting was carried out in the energy-band $0.5\text{--}7.0$ keV. The spectra were rebinned to ensure a S/N ratio of at least 3 and a minimum of 20 photons per bin (to validate χ^2 fitting). We fitted data from all annuli simultaneously using *Xspec*. To model the hot gas we adopted a *vaptec* component, plus a thermal bremsstrahlung component to account for undetected point-sources (this model gives a good fit to the composite spectrum of the detected sources in nearby galaxies: Irwin et al. 2003). In common with our previous anal-

ysis (Humphrey & Buote 2006a; Humphrey et al. 2006) we adopted a slightly modified form of the *Xspec* *vaptec* code to enable us to tie the ratio of each elemental abundance with respect to Fe between each annulus, while the Fe abundance (Z_{Fe}) was allowed to fit freely. To improve S/N Z_{Fe} was tied between adjacent annuli where constraints in individual annuli were poor. We allowed the global ratios of O, Ne, Mg, Si, S, and Ni with respect to Fe to fit freely, and fixed the remaining ratios at the Solar value (Asplund et al. 2004). The absorbing column density (N_{H}) was fixed at the Galactic value (Dickey & Lockman 1990). To account for projection effects, we used the *project* model implemented in *Xspec*. Since the X-ray emission appears truncated at large radius, we did not include a component to account for projection from outside our outermost annulus. However, as NGC 4649 is within the Virgo cluster, we took account of possible interloper cluster emission by including an additional hot gas component, with kT fixed at 2.5 keV (e.g. Gastaldello & Molendi 2002), which was assumed to have a constant surface brightness over the field of view. We obtained a reasonable fit ($\chi^2/\text{dof}=1178/1088$) to the spectra with this model, which is of comparable quality to our previous analysis of 7 systems (Humphrey et al. 2006). The best-fitting abundances were in agreement with those reported for NGC 4649 in that paper. Error-bars were computed *via* the Monte-Carlo technique outlined in Humphrey et al. (2006), and we carried out 50 error simulations. The resulting temperature and density profiles are discussed below.

3. MASS MODELLING

3.1. Entropy-Temperature method

In our previous work (Humphrey et al. 2006; Gastaldello et al. 2007; Zappacosta et al. 2006) we considered a variety of different approaches to solve the equation of hydrostatic equilibrium and obtain the mass profile. In our past analysis of NGC 4649, we adopted a parameterized model for the total gravitating mass profile and an ad hoc model for the temperature profile, solving for the total gas density. Although this method allowed us to obtain interesting constraints, it relies to some extent on the adoption of a temperature profile with reasonable asymptotic behaviour. We found a wide range of different temperature profiles for the galaxy-scale objects in our sample, unlike the approximately “universal” temperature profiles of galaxy clusters and, to some extent, galaxy groups (Vikhlinin et al. 2005; Gastaldello et al. 2007; Rasmussen & Ponman 2007).

As an alternative to these methods, in the present work we chose to exploit the fact that the *entropy* profile is, in general, far smoother than the temperature or density profiles and can typically be fitted by simple parameterized models which are well-behaved asymptotically (e.g. Donahue et al. 2006). In what follows we define the quantity $S = \rho^{-2/3}kT/(\mu m_{\text{H}})$, where ρ is the gas density, T is the temperature, k is Boltzmann’s constant, m_{H} is the mass of a hydrogen atom and μ is the mean molecular weight factor, taken to be 0.62. This is related to the actual entropy by a logarithm and multiplicative constant and is proportional to the usual “entropy” proxy used in the literature, $s = n_e^{-2/3}kT$ (e.g. Sanderson et al. 2003). An advantage of considering the entropy profile

is that stability against convection requires dS/dr to be positive at all radii, if the hydrostatic equilibrium equation is valid, placing a further constraint on meaningful models and improving our mass constraints.

One can write the equation of hydrostatic equilibrium in terms of pressure, P , and S as

$$\frac{dx}{dr} = -\frac{2}{5} \frac{GM_{TOT}(r)}{r^2} S^{-3/5} \quad (1)$$

where $x=P^{2/5}$, G is the universal gravitating constant, and $M_{TOT}(r)$ is the total mass enclosed within a given radius r . For a given distribution of S and M_{TOT} , this equation can be directly solved for x , provided the mass contribution of the gas can be neglected at all radii. Although this is true in the present work, since the gas contributes $< 1\%$ of the mass at all radii, in practice we allowed for a nonzero gas mass by differentiating and rearranging the equation to give:

$$\frac{d}{dr} \left(r^2 S^{3/5} \frac{dx}{dr} \right) + \frac{8G\pi r^2}{5S^{3/5}} x^{3/2} = -\frac{2}{5} G \frac{dM}{dr} \quad (2)$$

where the mass enclosed, M , comprises only the dark matter, stellar mass and the black hole mass. The gas mass is represented by the second term on the left hand side. For any parameterized distributions of S and M , this equation can be solved uniquely for x using a Runge-Kutta method. This means that for any such parameterized models of mass and entropy, the temperature and density profiles can be uniquely determined. We began all integrations at 10 pc, assuming the gas contributes negligibly to the total mass within this radius. The starting value for x (i.e. central pressure) at 10 pc was determined as a free parameter of our fit.

For each annulus in which we extracted data, we explicitly integrated appropriately weighted functions of pressure and temperature to compute the predicted contribution to the emission measure (and hence mean density) from gas in the corresponding shell (recalling that the data have been deprojected). We also computed an emission-weighted temperature (ignoring the temperature and abundance dependence of the emissivity, since neither term varies much over the field of view). We compared these averaged quantities to our measured temperature and density data-points. See Gastaldello et al. (2007, Appendix B) for a detailed discussion of incorporating the plasma emissivity into the gas modelling.

3.2. The stellar mass component

In order to place constraints on the black hole mass in the centre of a galaxy, it is imperative that we have an accurate picture of the stellar mass in that region. To do this, we assumed that the stellar mass follows the three dimensional distribution of the optical light, provided we adopt data observed in as red a filter as possible. From our Lick index analysis (Humphrey et al. 2006), we were able to estimate a mean age for the stellar population, as well as both a central stellar abundance and an emission-weighted abundance for the galaxy as a whole. Adopting the stellar population models of Maraston (2005), the J-band M/L_J ratio should only change by $\sim 3\%$ depending on which of the two abundances is assumed. This supports the assumption that mass follows light. To ensure maximum accuracy at the scale

of our innermost *Chandra* data-bins, we first considered the HST WFPC2 data with the F814W (approximately I-band) filter (for more details on the HST analysis see Humphrey 2007). We considered only data on the PC chip (to prevent the particular geometry of the WFPC2 plane complicating our analysis), limiting our profile to a radius of $\sim 11''$. To extend the coverage to larger radii ($\sim 4'$), we adopted the publicly-available 2MASS J-band images, masking out all data within the D_{25} ellipse (as listed in de Vaucouleurs et al. 1991) of the interloper spiral galaxy NGC 4647 (Fig 1) as well as from the vicinity of any bright point-sources. Although we were not able exactly to match the filters used in both cases, when the I-band HST profile is suitably rescaled, the profiles agree well outside $\sim 2''$, implying that there is not a strong I-J colour gradient over the HST field of view, and hence we can use the HST data as a proxy for a high-resolution J-band image.

By visual inspection, the axis ratio (major/minor) of the optical isophotes is $\lesssim 1.2$ at all radii of interest (Fig 1), indicating that the galaxy is fairly round; in what follows we adopt a spherical approximation. First we investigated whether simple analytical models can adequately match the observed surface brightness profile. We found that the de Vaucouleurs model significantly over-estimated the optical light in the centre of the galaxy. A Sersic profile with $n \simeq 2.6$ was able to characterize the overall shape of the profile but, especially in the inner regions, could not capture its fine detail (Fig 2).

Rather than using these simple prescriptions, we instead adopted a numerical deprojection technique, which is justified given the high quality of the data. We divided the emission into a series of concentric shells with outer and inner radii corresponding to the annuli in which our surface brightness profile (Fig 2) was computed. In each shell, we assumed the luminosity density of the stars was constant, enabling us to relate the observed surface brightness in each annulus to an appropriately weighted sum of emission from the shell it intersects and those outside it (e.g. Kriss et al. 1983). We assumed there was no emission outside the outermost shell, allowing us to compute the luminosity density (in $L_\odot \text{ kpc}^{-3}$) in the last shell directly from the measured surface brightness in our outer annulus. We then stepped inwards, iteratively solving for the luminosity in each shell. This technique is effectively the same as the ‘‘onion peeling’’ algorithm widely used to deproject spectra (e.g. Buote 2000). We assumed a J-band solar magnitude of 3.71, for consistency with the stellar population models of Maraston (2005). We have confirmed that the integrated light profile is in good agreement with the V-band deprojected light profile used by Gebhardt et al. (2003) (when scaled by a factor 3.34 which, using Maraston’s models, accounts for the different photometric bands used given the metallicity and age of the stars in the centre of NGC 4649). The profiles differed by less than 20% over all scales at which they overlapped, and typically agreed within a few percent (especially in the crucial inner kpc). Such agreement provides further support for our assumption that the stellar M/L_J ratio is approximately constant with radius.

4. RESULTS

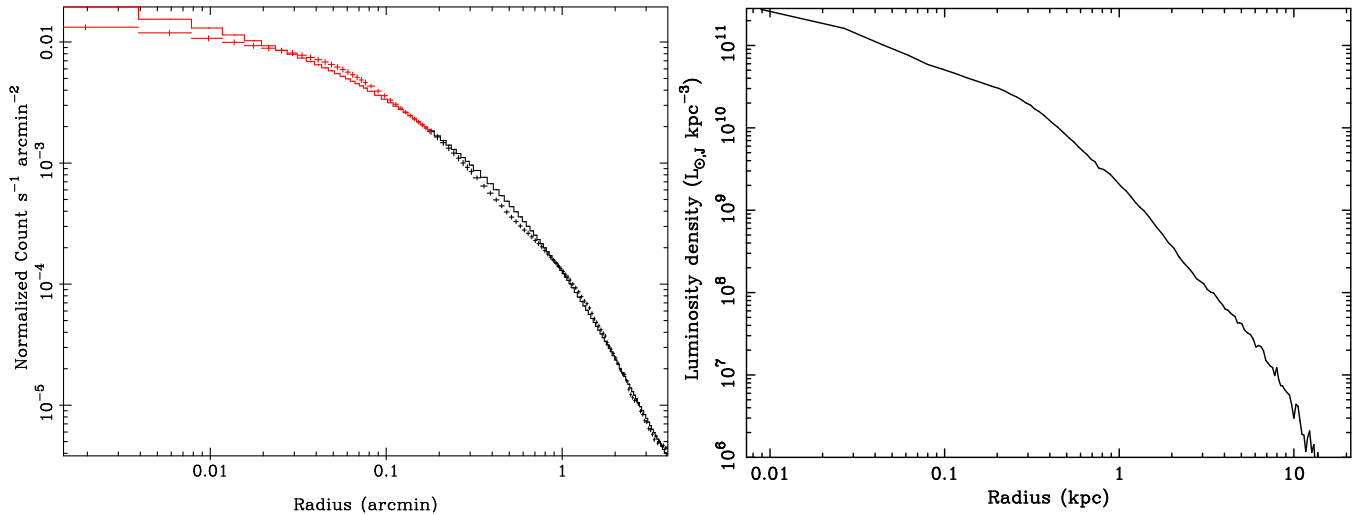


FIG. 2.— *Left*: Surface brightness profile of the galaxy, in optical light, shown with the best-fitting Sersic model. The Sersic model describes the overall shape, but not the detail of the luminosity profile. To aid the fitting, a systematic error of 5% has been added in quadrature with the statistical errors on each data-point. The J-band 2MASS profile is shown in black, and the renormalized I-band HST data in red. *Right*: The non-parametrically deprojected J-band luminosity density profile.

TABLE 2
THE BEST-FIT RESULTS

Parameter	Value
χ^2/dof	18.3/20
M_{BH}	$(3.35^{+0.67}_{-0.95}) \times 10^9 M_{\odot}$
stellar M/L_J	$1.37 \pm 0.10 M_{\odot} L_{\odot}^{-1}$
s_0	$2.00^{+0.26}_{-0.37} \text{ keV cm}^2$
s_1	$8.6^{+2.3}_{-1.4} \text{ keV cm}^2$
β_1	1.5 ± 0.18
s_{brk}	$2.44^{+0.59}_{-0.40} \text{ kpc}$
β_2	1.07 ± 0.05

NOTE. — Selected best-fitting parameters (see text).

From our spectral-fitting results, we have determined mean temperature and density data-points within each annulus. We converted these data to a mean (emission-weighted) entropy profile, as shown in Fig 3. We chose to fit this profile with a simple empirical model, for which we found a broken-powerlaw plus a constant model to be sufficient, i.e.:

$$s = s_0 + s_1 f(r) \quad (3)$$

where:

$$f(r) = \left(\frac{r}{s_{brk}} \right)^{\beta_1} (r < s_{brk})$$

$$\left(\frac{r}{s_{brk}} \right)^{\beta_2} (s_{brk} \leq r) \quad (4)$$

As explained in § 3, for a pair of parameterized models for entropy and the mass profile, one can uniquely determine the temperature (and density) profile. It is therefore possible to determine the best-fitting parameters of the mass model by fitting the entropy and temperature data simultaneously, while varying the parameters which describe the entropy and mass profiles. Since the fractional error-bars on the density are typically far larger than those on the temperature (due to partial degeneracies between the continuum and the unresolved point-source component, and between the gas density

and abundance, for the range of temperatures considered here), we found this was more constraining than fitting, for example, entropy and pressure at the same time.

To model the mass profile, in addition to the mass of the gas we included a stellar mass component, as described in § 3.2, an NFW dark matter model, following Navarro et al. (1997), and a central supermassive black hole. We allowed the stellar mass-to-light (M/L_J) ratio, central black hole mass (M_{BH}), and total mass and concentration of the NFW dark halo to fit freely. We find that the global parameters of the dark matter (NFW) halo are highly degenerate with each other without the application of additional constraints (e.g. Humphrey et al. 2006), but their exact values have little bearing on the shape of the dark matter profile in the region of interest, so we will discuss them in detail in a future paper.

Because the measured entropy and temperature in each annulus were, by definition, averaged quantities, in contrast to the continuous, parameterized functions being fitted, care was taken over comparing the model with the data. The model density profile (squared) was explicitly integrated over each bin to compute the emission measure, while the temperature model was similarly integrated with ρ_{gas}^2 (emission) weighting. These quantities correspond to the observables determined directly from the spectral fitting, and so could be used to compute the emission-weighted entropy (and temperature) for direct comparison with the data. The best-fitting entropy model is shown in Fig 3, and exhibits asymptotic (large radius) behaviour consistent with the expected $s \propto r^{1.1}$ from structure formation models incorporating purely gravitational processes (e.g. Tozzi & Norman 2001). We also show the temperature and gas density profiles of the object, along with the best-fitting models in Figs 4 and Fig 5.

The radial dependence of the best-fitting mass model is shown in Fig 6, along with the contribution of each of the separate mass components. We find that the stellar mass component dominates the mass profile within ~ 6 kpc, with a significant contribution of dark matter

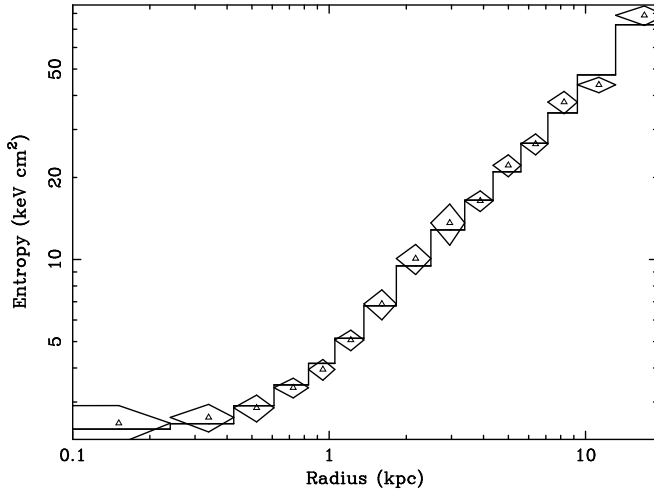


FIG. 3.— The entropy profile of the data, shown along with the best-fitting model. Although the profile flattens at small radii the entropy gradient is always positive, as expected for gas in hydrostatic equilibrium.

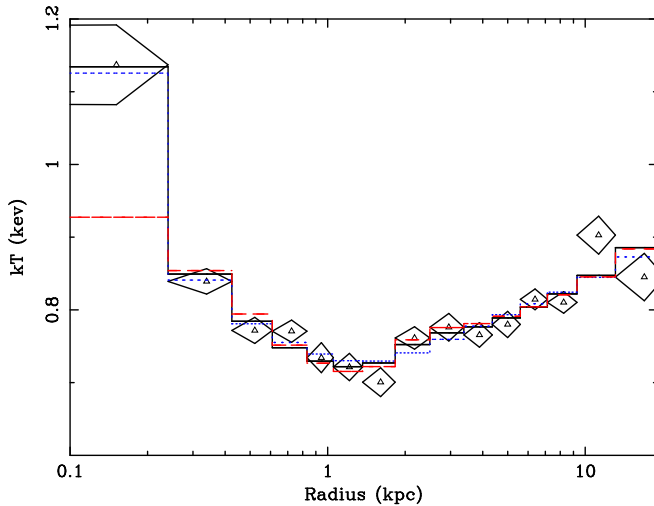


FIG. 4.— Measured temperature profile of the hot gas in NGC 4649 (error diamonds). Also shown are the best-fitting modelled profile from the entropy-temperature analysis (solid line; black) and the best-fitting temperature profile if a central black hole is omitted (dashed line; red). In addition, the dotted line (blue) indicates the best-fitting arbitrary parameterized model (See § 4.1).

required to explain our observations at large radii. This is largely consistent with our previous analysis, despite the much simpler stellar mass profile we adopted in that work. Within our innermost annulus, however, we found that the rapidly-falling stellar mass was unable to explain the strong peak in the temperature profile. We show in Fig 4 the best-fit temperature model with the black hole mass (M_{BH}) fixed at zero, which clearly does not reproduce the sharp central spike and is only a marginally acceptable fit (global $\chi^2/\text{dof}=33.7/21$). Allowing the black hole mass to fit freely enabled us to obtain an excellent fit to the data ($\chi^2/\text{dof}=18.3/20$), an improvement significant at 99.94% significance, based on an f-test. The best-fitting values of key fit parameters are shown in Table 2.

4.1. Traditional mass analysis

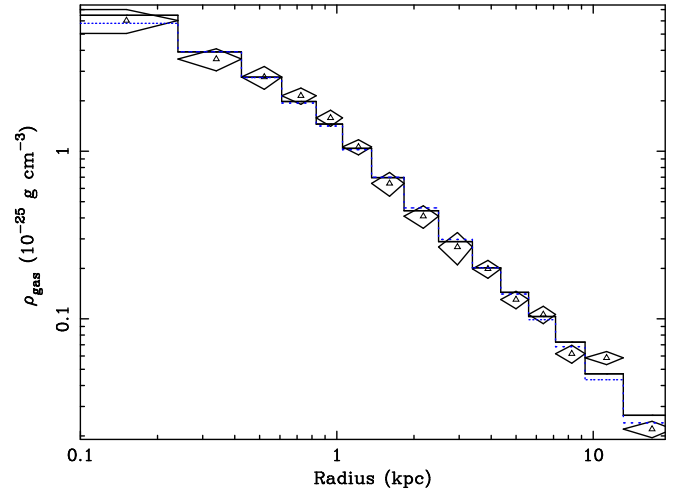


FIG. 5.— Measured gas density profile of the hot gas in NGC 4649 (error diamonds). Also shown are the best-fitting modelled profile from the entropy-temperature analysis (solid line; black) and the best-fitting arbitrary parameterized model (dotted line; blue. See § 4.1).

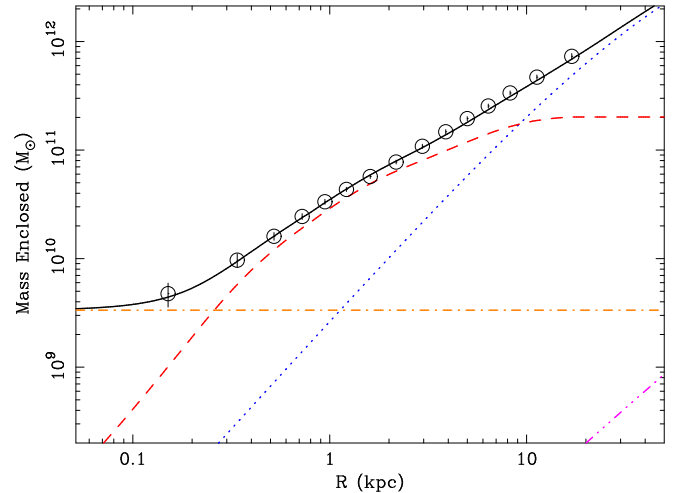


FIG. 6.— Mass profile of NGC 4649 determined from our fitting. The individual data-points were derived from the traditional non-parametric method discussed in Gastaldello et al. (2007). We also show our best-fitting mass-profile determined from our entropy-temperature modelling method (see text). We show separately the total mass enclose (solid line; black), the stellar component (dashed line; red), the dark matter (dotted line; blue), the gas (dash-dot-dot-dot line; magenta) and the black hole mass (dash-dot line; orange). We stress that the models *do not* represent a fit of the data-points, which were derived independently.

In our analysis, we adopted a new approach to X-ray mass analysis, which we expect to give a more precise determination of M_{BH} than would be expected from other, more traditional approaches. However, it is also of interest to determine whether interesting results can be obtained using the older methods, which have the advantage of less computational expense. In order to investigate this, we additionally analysed the data using a more orthodox mass-analysis approach (here dubbed the “traditional method”). In this case, we adopted ad hoc parameterized models for both the temperature and density profiles. These models were chosen to capture as much detail of the profiles as possible, but may not be a perfect fit to the data. One can simply compute

TABLE 3
SYSTEMATIC ERROR BUDGET

Test	M_{BH} ($10^9 M_{\odot}$)	M/L_J ($M_{\odot} L_{\odot}^{-1}$)
Best-fit	3.35	1.37
$\Delta\text{Statistical}$	$+0.67$ -0.95	± 0.10
ΔMethod	$+0.75$	-0.13
$\Delta\text{Distance}$	$+0.01$ -0.27	$+0.06$ -0.12
$\Delta\text{Plasma code}$	$+0.11$	-0.07
$\Delta\text{Bandwidth}$	-0.61	$+0.06$
ΔXRB	0.005	0.001
ΔN_{H}	0.001	0.001
$\Delta\text{Background}$	-0.10	$+0.22$
$\Delta\text{Centroiding}$	0.001	0.02
$\Delta\text{Asymmetry}$	$+0.16$	-0.002

NOTE. — Summary of the error-budget for the mass analysis. We list the best-fitting values of M_{BH} and mass-to-light (M/L_J) and the (90%) statistical errors ($\Delta\text{Statistical}$). In addition we show estimates of the magnitude of the systematic uncertainties due to various factors. These should not be added in quadrature with the statistical errors. We show the impact of adopting different fitting methods (ΔMethod ; see text), the estimated errors due to distance errors ($\Delta\text{Distance}$), uncertainties in the plasma code ($\Delta\text{Plasma code}$), the choice of bandwidth ($\Delta\text{Bandwidth}$), modelling of unresolved X-ray binaries (ΔXRB), the adopted N_{H} (ΔN_{H}), treatment of the background ($\Delta\text{Background}$), centroiding errors ($\Delta\text{Centroiding}$), and possible asymmetry in the data ($\Delta\text{Asymmetry}$).

the mass enclosed within any radius by differentiating these models and inserting the derivatives into an appropriately re-arranged form of the hydrostatic equilibrium equation. We used this approach to generate mass “data-points” corresponding to each of our annuli. We discuss this method, and the models we used to fit our data, in detail in Gastaldello et al. (2007).

For our present analysis, we fitted the density profile with a standard beta-model functional form, with an added central cusp. To fit the complicated temperature profile, we adopted a model comprising two smoothly-joined powerlaws. We show the fits to each profile in Figs 4 and 5, and the mass data-points are overlaid on our best-fitting mass model in Fig 6. Clearly, there is excellent agreement between these two profiles, indicating the robustness of our mass analysis results. There are, nonetheless, slight differences if we fit the mass data-points directly with our parameterized mass model (we omitted the gas mass, which is negligibly small over the range of interest), in large part because our adopted temperature profile does not fully capture the curvature of the data around 1–2 kpc. Nonetheless, from these data we found $M_{\text{BH}} = (4.1 \pm 2.2) \times 10^9 M_{\odot}$, which, although slightly higher than our best estimate, is statistically consistent with it. It is also within 1.6σ of the stellar kinematical estimate of Gebhardt et al. (2003). Similarly, our measured M/L_J ratio, $1.24 \pm 0.22 M_{\odot} L_{\odot}^{-1}$ was slightly discrepant, but statistically consistent, with our preferred value.

5. SYSTEMATIC ERROR BUDGET

In this section we address the sensitivity of our results to various data-analysis choices which were made. We focused on those systematic effects we estimate to be most likely to affect our results. An estimated upper limit on the sensitivity of our results to these choices is shown

in Table 3. These numbers reflect the sensitivity in the best-fit parameter to each potential source of systematic error, and we stress they should *not* be added in quadrature with the statistical errors. We outline below how each test was performed. Those readers uninterested in the technical details of our analysis may wish to proceed directly to § 6.

First of all, in Table 3, we list (ΔMethod) the impact of using the traditional mass analysis method described in § 4.1, as opposed to the default method we adopted. The traditional method is limited in that the adopted parameterized models have difficulty in capturing the fine details of the temperature and density profiles. Nonetheless, the results are in good agreement from both techniques. Next we investigated the impact of changing the distance by ± 1.8 Mpc, corresponding approximately to the 90% statistical error the I-band SBF distance measurement of Tonry et al. (2001). This range encompasses the adopted distance (16.8 Mpc) used by Gebhardt et al. (2003). This had only a minimal impact on the measured M_{BH} , although more effect on the M/L_J ratio.

We next considered whether our spectral-fitting choices could have led to a systematic mis-estimation of the density and temperature, and hence M_{BH} . There are some uncertainties in the modelling of individual emission lines, in particular for the important Fe blend, so we therefore experimented with replacing the APEC plasma model with the MEKAL code, which models the atomic physics differently. This had only a slight impact on the best-fit results ($\Delta\text{Plasma code}$). To assess whether the adopted bandwidth can affect our results, we experimented with fitting the data in the ranges 0.7–7.0, 0.5–2.0 keV and 0.4–7.0 keV, in addition to the default 0.5–7.0 keV. We estimated the impact on our results of improperly modelling the unresolved X-ray binary spectral component by varying the temperature of the parameterized (bremsstrahlung) model by $\pm 25\%$, or replacing it with a powerlaw with $\Gamma=1.5$. Finally, to determine whether systematic errors in the adopted absorbing column could lead to a large error on M_{BH} , we perturbed N_{H} by $\pm 25\%$ from its nominal value (Dickey & Lockman 1990).

A potentially serious cause for concern when performing spectral analysis of diffuse emission is the treatment of the background. We therefore investigated whether our choice for the background made an impact on our results by adopting, instead of our preferred treatment given in § 2.2, spectra extracted from appropriately projected background template events files distributed with the *Caldb*. These template files are constructed from processed, stacked observations of nominally blank-sky fields. Although they do not directly take into account the large-scale variation in the cosmic X-ray background (nor variability in the non X-ray background component), they are widely used to estimate the background in *Chandra* analysis. The templates were renormalized to ensure the 9.5–12 keV count-rates of the source and the background agreed; this is formally incorrect since it also renormalizes the cosmic X-ray background in the templates as well. Nonetheless, we found that the choice of background did not have a significant impact on M_{BH} , although the systematic effect on M/L_J is larger than the statistical errors. This is easily understood since M_{BH} is determined by data from the bright, central regions of

the galaxy, where the background is negligible.

Another possible cause of systematic error in our analysis is improper centroiding; if our spectral extraction regions were offset from the dynamical centre of the galaxy, this will cause the derived temperature and density profiles to be systematically incorrect, leading to an error in the computation of the central mass. In practice, we would expect a mis-alignment to result in a systematically under-estimated central temperature, reducing the significance of the SMBH detection. We checked the agreement of the *Chandra* centroid and the optical centre (identified by eye from the HST images); based on a bootstrap alignment of the *Chandra* and HST images, which required a fraction of the point sources in each to match (Humphrey & Buote 2006b), we estimated they are consistent within $\sim 0.6''$, which is comparable to the on-axis PSF of *Chandra*. We found that moving the X-ray centre by this amount made little difference to our overall result (Δ Centroiding), which is unsurprising since the shift is very much smaller than the radius of the central extraction region ($2.5''$).

Finally, we considered whether low-level asymmetries in the X-ray image might constitute a strong deviation from our assumption of spherical symmetry. To investigate the possible impact of such features, we artificially restricted the field of view, re-extracting all spectra from a set of suitably-oriented concentric semi-annuli. We found the fit results agreed very well with our best-fit, indicating that any such asymmetries, if present, only have a minor impact. It is worth noting that, if the system globally deviated strongly from hydrostatic equilibrium, it would be highly unlikely that we would observe such symmetry.

6. DISCUSSION

Using the assumptions of hydrostatic equilibrium, spherical symmetry, a single-phase ISM and that the stellar mass follows the optical light, we have obtained an estimate for the mass of the supermassive black hole at the centre of NGC 4649⁷. This is the first time that the mass of a supermassive black hole has been determined from the distribution of hydrostatic, X-ray emitting gas. In principle, this method can also be applied to other giant elliptical galaxies with relaxed X-ray morphologies, allowing the most massive black holes to be studied.

We placed a lower limit on the black hole mass of $1.6 \times 10^9 M_\odot$, at 99% confidence. Our measured mass agrees (within $\sim 2\sigma$) with that determined from stellar kinematical studies, $(2.0^{+0.4}_{-0.6}) \times 10^9 M_\odot$ (1σ error), based on a different set of assumptions. This makes NGC 4649 one of only a handful of galaxies for which M_{BH} has been measured *via* multiple complementary methods. Although the overall agreement in the shape of the $M_{\text{BH}}\text{-}\sigma_*$ relation when measured using different techniques (e.g. Gebhardt et al. 2000b) provides good evidence that the masses from stellar kinematics are not *on average* in error, the systematic uncertainties on any

individual measurement of M_{BH} are more difficult to assess. In the few systems where the mass can be inferred from both gas and stellar dynamics, the results have been mixed, possibly on account of non-circular gas motions (§ 1). Therefore, the good agreement we found between the measurements of M_{BH} from stellar dynamics and hydrostatic gas analysis provides crucial, independent verification that stellar dynamics can be used to determine reliable SMBH masses, and effectively rules out pathological orbital structure for the central part of NGC 4649.

Our results provide strong support not only for the stellar kinematical results but also the single-phase, hydrostatic equilibrium approximation we adopted. Firstly, the X-ray image shows a remarkably symmetrical morphology; we do not confirm the evidence of significant asymmetries previously reported with shallower data (Randall et al. 2004; Shurkin et al. 2008). Secondly, the hydrostatic mass model actually fits the data remarkably well, despite the complicated temperature and density profiles. Thirdly, we find good agreement between M_{BH} determined *via* both optical and X-ray techniques. As our derived mass profile was extended to larger radii, we found excellent agreement with stellar mass profile within ~ 3 kpc. At even larger radii, the mass determination from the kinematics of globular clusters agreed very well with our results (Bridges et al. 2006). Taken together, these indicate that the ISM NGC 4649 must be very close to hydrostatic equilibrium at all scales, or there is a remarkable conspiracy in the data.

In a recent provocative paper, Diehl & Statler (2007) analysed the X-ray morphology of a sample of early-type galaxies and concluded that, since the majority show clear evidence of morphological disturbances in their cores, probably all elliptical galaxies are out of hydrostatic equilibrium. Quite apart from the obviously false syllogism that, since there exists disturbed (non-hydrostatic) ISM in many early-type galaxies, *all* early-type galaxies (including those without clear disturbances) are non-hydrostatic, NGC 4649 represents a clear counter-example to this argument. This is unsurprising, since cosmological simulations of galaxy clusters have shown that the existence of asymmetries typically does not translate to mass errors of more than 25% (Tsai et al. 1994; Evrard et al. 1996; Nagai et al. 2007), even in systems that are manifestly more disturbed than NGC 4649. Comparing optical and X-ray mass estimates for two systems (NGC 1399 and M87) that are much more disturbed than NGC 4649, a recent study by Churazov et al. (2007) reaches a similar conclusion. Hence, even when low-level asymmetrical features are eventually detected with higher quality data, as they must, there is no evidence from either theoretical or observational studies that this implies a systematic error in the derived mass much larger than the other systematic errors we addressed in this paper.

With *Chandra* we were unable to resolve the sphere of influence (~ 60 pc) of the SMBH on the gas although, since the emissivity is proportional to the square of the gas density (which rises steeply towards the centre), we were able to probe the gas density within a factor $\sim 2\text{--}3$ of it. Provided hydrostatic equilibrium holds, resolving the sphere of influence is not strictly necessary to place constraints on the central mass if one takes care to compute reliable average densities and temperatures within

⁷ We note that, technically we also require the entropy profile not to behave pathologically at small radii. However, since hydrostatic equilibrium requires $dS/dr > 0$, the most discrepant behaviour we might expect to see in S is a precipitous drop. In such a case, this would tend to *reduce* a central peak in the model temperature profile, making the evidence for a supermassive black hole even stronger.

each radial bin. Ideally, however, X-ray imaging spectroscopy at scales smaller than this scale is desirable so that the SMBH mass is not determined primarily by a single data-point. With such data one could also search for morphological disturbances at the smallest scales, which would indicate local deviations from hydrostatic equilibrium. Unfortunately, such imaging is beyond the capabilities of *Chandra* and will have to wait until the era of higher spatial resolution X-ray instruments. Nonetheless, within the central ~ 200 pc, the dynamical time-scale is only 8×10^5 yr, as compared to a cooling time $\sim 2 \times 10^7$ yr so that, unless the gas is being constantly stirred up, we would expect it to relax quickly into a state approximating hydrostatic equilibrium. Although ISM disturbances due to AGN activity appear common in early-type galaxies (e.g. Jones et al. 2002), these are typically seen on large scales, comparable to any radio lobes (which, although very weak in NGC 4649, are on \sim kpc scales: Stanger & Warwick 1986). Given that the dynamical time-scale is shortest in the central parts of the galaxy, NGC 4649 would have to be in a very unusual state for AGN activity to stir up the gas within only the central ~ 100 pc but leave the X-ray morphology outside this range undisturbed. Although the current X-ray data do not allow us completely to rule this out, turbulence or bulk motion would provide additional support against gravity (e.g. Nagai et al. 2007), lowering the central temperature for a given mass and entropy, and leading to an underestimate of M_{BH} . Since a deviation from this assumption would lead to poorer agreement with the optical data, our results indicate that the gas is very close to hydrostatic.

In addition to being close to hydrostatic equilibrium, our results indicate that the gas must also be close to single phase. We tested this explicitly by adding an extra **vap**ec spectral component in each annulus. We found that the fit did not improve significantly ($\Delta\chi^2=9$ for 30 fewer degrees of freedom) and, excepting the innermost bin, the extra component was negligible in each annulus, supporting the single-phase assumption. Although we cannot rule out multi-phase gas within the innermost ~ 200 pc, it is difficult to understand why genuinely multi-phase gas would be confined only to this region. Fitting a single temperature model to data where multi-temperature models are actually required in general should lead us to underestimate the mass (e.g. Allen 1998), so, if anything, the effect of multi-phase gas would be to make our measured M_{BH} more discrepant with the optical data (implying the gas is probably single-phase). It is worth noting that our models do indicate a steeply-rising temperature profile within the innermost bin and in such cases, two-temperature spectral models are often statistically better descriptions of the data than single-temperature models (e.g. Buote 2000). However, one can still obtain reliable mass profiles by interpreting a single-temperature fit to the data provided one takes care to compare its parameters to a suitably averaged model, as we did in the present work (Gastaldello et al. 2007).

One of the intriguing results from our analysis is an explanation of the central temperature spike seen in this system. As we show in Fig 4, if we omit the central black hole, our model temperature profile is much less centrally-peaked than the real data. This confirms the predictions of Brighenti & Mathews (1999), who

suggested that such features should be prevalent when *Chandra* temperature profiles of elliptical galaxies hosting massive black holes are investigated. This detection, therefore, opens the possibility of using the same technique to measure the central black hole mass in other, morphologically relaxed, early-type galaxies. Since significant X-ray halos are most often associated with the most massive galaxies, this will make such a method particularly sensitive to the most massive black holes. However, even for a black hole as massive as $\sim 3 \times 10^9 M_{\odot}$, the sphere of influence is only ~ 50 pc, requiring precise temperature constraints on a comparable scale. Within the limitations of current instrumentation, this effectively restricts the analysis to very X-ray bright galaxies within ~ 20 Mpc, severely limiting the number of systems in which we might hope to see it. With the improved spatial resolution promised by proposed future X-ray satellites, such as the *Generation-X* mission (Windhorst et al. 2006), though, such measurements should become routine.

In practice, the presence of a central temperature spike is not actually a sufficient diagnostic for a massive central black hole. As is clear from Fig 4, a mild central increase in the temperature can arise as a consequence of the centrally-peaked stellar mass distribution. In fact, if the stellar mass was significantly more cuspy (for example in a “powerlaw” galaxy, rather than the “cored” NGC 4649), we would have seen a significant central temperature rise even without a black hole. More importantly, the mass profile alone does not determine the shape of the temperature profile, but instead it is the interplay of the mass and entropy profiles. The shape of the latter is set by the balance between heating and cooling, which is not completely understood. In general, the flatter the central entropy profile, the more centrally-peaked is the temperature profile, so quantitative differences in the thermal histories of individual galaxies would explain in part the paucity of such temperature spikes. In many objects, this is compounded by the presence of AGN-driven disturbances (e.g. Bîrzan et al. 2004; O’Sullivan et al. 2005), which tend to stir up the gas, disturbing hydrostatic equilibrium and mixing hot, central gas with cooler gas from larger radii. Combined with the observational difficulty of the measurement, these effects may explain the few reported galaxies exhibiting this feature (e.g. Humphrey et al. 2006, 2004), in contrast to the ubiquity of black holes.

In addition to the black hole mass estimate, our method also allowed us to determine directly the total stellar mass of the system, without making any assumptions regarding the stellar mass-to-light ratio, and requiring only that stellar mass follows light. We therefore obtained *both* data-points (albeit not completely independently) to place on a M_{BH} *versus* stellar mass relation. We estimated that the mass of the SMBH is $\sim 1.7\%$ times the mass in stars of the galaxy. It is interesting to compare this to the relations between M_{BH} and bulge mass (M_{bul}) found by Marconi & Hunt (2003). For a bulge mass of $\sim 2 \times 10^{11} M_{\odot}$, those authors would predict a ratio of M_{BH} to M_{bul} of $\sim 0.2\%$, which is discrepant at almost an order of magnitude from our measurement (larger than the expected scatter). Marconi & Hunt estimated M_{bul} by inserting the stellar velocity

dispersion and effective radius into the Virial relation, which actually gives an estimate of the *total* gravitating matter within, roughly, the effective radius. For the case of NGC 4649, which they include in their sample, they adopted an effective radius of 7.5 kpc (corrected to our adopted distance) and derived $M_{\text{bul}} \simeq 7.8 \times 10^{11} M_{\odot}$. This is considerably higher than the *stellar* mass we measured within the galaxy and, not unexpectedly, falls far short of the $\sim 3 \times 10^{13} M_{\odot}$ Virial mass of the entire system (Humphrey et al. 2006). Instead, this is approximately the total gravitating mass within ~ 19 kpc, of which dark matter comprises almost $\sim 75\%$. Clearly this illustrates the difficulty in interpreting Virial theorem estimates for M_{bul} , especially at the most massive end where galaxies sit in the centres of group-like dark matter halos. In order to gain insight into the SMBH-bulge relation, a full decomposition of the mass profile into stellar and dark components is, therefore, essential.

Finally, based on the mean stellar population age and abundance estimated from our Lick index analysis (Humphrey et al. 2006), we can estimate the expected mass-to-light (M/L_J) ratio for different simple stellar population models, assuming all stars were born in a swift burst of star-formation. Using the models of Maraston (2005), the J-band ratio is $1.86 \pm 0.21 M_{\odot} L_{\odot}^{-1}$, assuming a Kroupa (2001) IMF, and depending only very weakly on the metallicity of the stars. As an alternative, if we adopt version 2 of the PEGASE code (Fioc & Rocca-Volmerange 1997), the predicted J-band M/L ratio is $1.55 \pm 0.16 M_{\odot} L_{\odot}^{-1}$, indicating the level of system-

atic uncertainty in such population models. These results compare favourably with our observed stellar M/L_J ratio ($1.37 \pm 0.10 M_{\odot} L_{\odot}^{-1}$), although the Maraston models are slightly discrepant. We note that our measured M/L_J is completely inconsistent with the predictions for a Salpeter IMF ($2.7 \pm 0.3 M_{\odot} L_{\odot}^{-1}$ for both sets of models), as we found in Humphrey et al. (2006), unless the age for the stellar population is dramatically over-estimated. In that case it would need to be closer to ~ 7 Gyr than the 13 ± 2 Gyr we measured.

We would like to thank Misty Bentz for useful discussions. Some of the data presented in this paper were obtained from the Multimission Archive at the Space Telescope Science Institute (MAST). STScI is operated by the Association of Universities for Research in Astronomy, Inc., under NASA contract NAS5-26555. This research has also made use of the NASA/IPAC Extragalactic Database (*NED*) which is operated by the Jet Propulsion Laboratory, California Institute of Technology, under contract with NASA. Partial support for this work was provided by NASA under grant NNG04GE76G issued through the Office of Space Sciences Long-Term Space Astrophysics Program. Partial support was also provided by NASA through Chandra Award Number G07-8083X issued by the Chandra X-Ray Center, which is operated by the Smithsonian Astrophysical Observatory for and on behalf of NASA

REFERENCES

- Allen, S. W. 1998, MNRAS, 296, 392
- Asplund, M., Grevesse, N., & Sauval, J. 2004, in Cosmic abundances as records of stellar evolution and nucleosynthesis, ed. F. N. Bash & T. G. Barnes (ASP Conf. series), astro-ph/0410214
- Binney, J. & Mamon, G. A. 1982, MNRAS, 200, 361
- Birzan, L., Rafferty, D. A., McNamara, B. R., Wise, M. W., & Nulsen, P. E. J. 2004, ApJ, 607, 800
- Bridges, T., Gebhardt, K., Sharples, R., Faifer, F. R., Forte, J. C., Beasley, M. A., Zepf, S. E., Forbes, D. A., Hanes, D. A., & Pierce, M. 2006, MNRAS, 373, 157
- Brighenti, F. & Mathews, W. G. 1999, ApJ, 527, L89
- Buote, D. A. 2000, ApJ, 539, 172
- Buote, D. A. & Canizares, C. R. 1994, ApJ, 427, 86
- Buote, D. A. & Tsai, J. C. 1995, ApJ, 439, 29
- Cappellari, M., Verolme, E. K., van der Marel, R. P., Kleijn, G. A. V., Illingworth, G. D., Franx, M., Carollo, C. M., & de Zeeuw, P. T. 2002, ApJ, 578, 787
- Churazov, E., Forman, W., Vikhlinin, A., Tremaine, S., Gerhard, O., & Jones, C. 2007, MNRAS, submitted, astro-ph/0711.4686
- Condon, J. J., Cotton, W. D., & Broderick, J. J. 2002, AJ, 124, 675
- Davies, R. I., Thomas, J., Genzel, R., Mueller Sánchez, F., Tacconi, L. J., Sternberg, A., Eisenhauer, F., Abuter, R., Saglia, R., & Bender, R. 2006, ApJ, 646, 754
- de Vaucouleurs, G., de Vaucouleurs, A., Corwin, H. G., Buta, R. J., Paturel, G., & Fouque, P. 1991, Third Reference Catalogue of Bright Galaxies (Volume 1-3, XII, 2069 pp. 7 figs.. Springer-Verlag Berlin Heidelberg New York)
- Di Matteo, T., Springel, V., & Hernquist, L. 2005, Nature, 433, 604
- Dickey, J. M. & Lockman, F. J. 1990, ARA&A, 28, 215
- Diehl, S. & Statler, T. S. 2007, ApJ, 668, 150
- Donahue, M., Horner, D. J., Cavagnolo, K. W., & Voit, G. M. 2006, ApJ, 643, 730
- Evvard, A. E., Metzler, C. A., & Navarro, J. F. 1996, ApJ, 469, 494
- Fang, T., Humphrey, P. J., & Buote, D. A. 2008, ApJ, submitted
- Ferrarese, L. & Ford, H. 2005, Space Sci. Rev., 116, 523
- Ferrarese, L. & Merritt, D. 2000, ApJ, 539, L9
- Ferrarese, L., Pogge, R. W., Peterson, B. M., Merritt, D., Wandel, A., & Joseph, C. L. 2001, ApJ, 555, L79
- Fioc, M. & Rocca-Volmerange, B. 1997, A&A, 326, 950
- Gastaldello, F., Buote, D. A., Humphrey, P. J., Zappacosta, L., Bullock, J. S., Brighenti, F., & Mathews, W. G. 2007, ApJ, 669, 158
- Gastaldello, F. & Molendi, S. 2002, ApJ, 572, 160
- Gebhardt, K., et al. 2000a, ApJ, 539, L13
- Gebhardt, K., et al. 2000b, ApJ, 543, L5
- Gebhardt, K., et al. 2003, ApJ, 583, 92
- Graham, A. W., Erwin, P., Caon, N., & Trujillo, I. 2001, ApJ, 563, L11
- Granato, G. L., De Zotti, G., Silva, L., Bressan, A., & Danese, L. 2004, ApJ, 600, 580
- Humphrey, P. J. 2007, ApJ, submitted
- Humphrey, P. J. & Buote, D. A. 2006a, ApJ, 639, 136
- Humphrey, P. J. & Buote, D. A. 2006b, ApJ, submitted, astro-ph/0612058
- Humphrey, P. J., Buote, D. A., & Canizares, C. R. 2004, ApJ, 617, 1047
- Humphrey, P. J., Buote, D. A., Gastaldello, F., Zappacosta, L., Bullock, J. S., Brighenti, F., & Mathews, W. G. 2006, ApJ, 646, 899
- Irwin, J. A., Athey, A. E., & Bregman, J. N. 2003, ApJ, 587, 356
- Jones, C., Forman, W., Vikhlinin, A., Markevitch, M., David, L., Warmflash, A., Murray, S., & Nulsen, P. E. J. 2002, ApJ, 567, L115
- Kormendy, J. 2004, in Coevolution of Black Holes and Galaxies, ed. L. C. Ho, 1
- Kormendy, J. & Richstone, D. 1995, ARA&A, 33, 581
- Kriss, G. A., Cioffi, D. F., & Canizares, C. R. 1983, ApJ, 272, 439
- Kroupa, P. 2001, MNRAS, 322, 231
- Lauer, T. R., et al. 2007, ApJ, 662, 808

- Macchetto, F., Marconi, A., Axon, D. J., Capetti, A., Sparks, W., & Crane, P. 1997, *ApJ*, 489, 579
- Magorrian, J., et al. 1998, *AJ*, 115, 2285
- Maraston, C. 2005, *MNRAS*, 362, 799
- Marconi, A. & Hunt, L. K. 2003, *ApJ*, 589, L21
- Marconi, A., Pastorini, G., Pacini, F., Axon, D. J., Capetti, A., Macchetto, D., Koekemoer, A. M., & Schreier, E. J. 2006, *A&A*, 448, 921
- Mathews, W. G. & Brighenti, F. 2003, *ARA&A*, 41, 191
- Mathews, W. G., Brighenti, F., & Buote, D. A. 2004, *ApJ*, 615, 662
- McLure, R. J. & Dunlop, J. S. 2002, *MNRAS*, 331, 795
- Miyoshi, M., Moran, J., Herrnstein, J., Greenhill, L., Nakai, N., Diamond, P., & Inoue, M. 1995, *Nature*, 373, 127
- Nagai, D., Vikhlinin, A., & Kravtsov, A. V. 2007, *ApJ*, 655, 98
- Navarro, J. F., Frenk, C. S., & White, S. D. M. 1997, *ApJ*, 490, 493
- Onken, C. A., Ferrarese, L., Merritt, D., Peterson, B. M., Pogge, R. W., Vestergaard, M., & Wandel, A. 2004, *ApJ*, 615, 645
- Onken, C. A., et al. 2007, *ApJ*, 670, 105
- O’Sullivan, E., Vrtilak, J. M., & Kempner, J. C. 2005, *ApJ*, 624, L77
- Peterson, B. M., et al. 2004, *ApJ*, 613, 682
- Randall, S. W., Sarazin, C. L., & Irwin, J. A. 2004, *ApJ*, 600, 729
- Randall, S. W., Sarazin, C. L., & Irwin, J. A. 2006, *ApJ*, 636, 200
- Rasmussen, J. & Ponman, T. J. 2007, *MNRAS*, 380, 1554
- Robertson, B., Hernquist, L., Cox, T. J., Di Matteo, T., Hopkins, P. F., Martini, P., & Springel, V. 2006, *ApJ*, 641, 90
- Sanderson, A. J. R., Ponman, T. J., Finoguenov, A., Lloyd-Davies, E. J., & Markevitch, M. 2003, *MNRAS*, 340, 989
- Shapiro, K. L., Cappellari, M., de Zeeuw, T., McDermid, R. M., Gebhardt, K., van den Bosch, R. C. E., & Statler, T. S. 2006, *MNRAS*, 370, 559
- Shurkin, K., Dunn, R. J. H., Gentile, G., Taylor, G. B., & Allen, S. W. 2008, *MNRAS*, 383, 923
- Silk, J. & Rees, M. J. 1998, *A&A*, 331, L1
- Stanger, V. J. & Warwick, R. S. 1986, *MNRAS*, 220, 363
- Tonry, J. L., Dressler, A., Blakeslee, J. P., Ajhar, E. A., Fletcher, A., Luppino, G. A., Metzger, M. R., & Moore, C. B. 2001, *ApJ*, 546, 681
- Tozzi, P. & Norman, C. 2001, *ApJ*, 546, 63
- Tremaine, S., et al. 2002, *ApJ*, 574, 740
- Tsai, J. C., Katz, N., & Bertschinger, E. 1994, *ApJ*, 423, 553
- Valluri, M., Merritt, D., & Emsellem, E. 2004, *ApJ*, 602, 66
- van der Marel, R. P., Cretton, N., de Zeeuw, P. T., & Rix, H.-W. 1998, *ApJ*, 493, 613
- van der Marel, R. P. & Franx, M. 1993, *ApJ*, 407, 525
- Verdoes Kleijn, G. A., van der Marel, R. P., de Zeeuw, P. T., Noel-Storr, J., & Baum, S. A. 2002, *AJ*, 124, 2524
- Vikhlinin, A., Markevitch, M., Murray, S. S., Jones, C., Forman, W., & Van Speybroeck, L. 2005, *ApJ*, 628, 655
- Windhorst, R. A., et al. 2006, *New Astronomy Review*, 50, 121
- Wyithe, J. S. B. 2006, *MNRAS*, 365, 1082
- Zappacosta, L., Buote, D. A., Gastaldello, F., Humphrey, P. J., Bullock, J., Brighenti, F., & Mathews, W. 2006, *ApJ*, 650, 777